Energy & Environmental Science

Cite this: *Energy Environ. Sci.*, 2011, **4**, 1288

www.rsc.org/ees

COMMUNICATION

Single-crystal ZnO nanorod/amorphous and nanoporous metal oxide shell composites: Controllable electrochemical synthesis and enhanced supercapacitor performances†

Yun-Bo He, Gao-Ren Li,* Zi-Long Wang, Cheng-Yong Su and Ye-Xiang Tong

Received 15th November 2010, Accepted 28th January 2011
DOI: 10.1039/c0ee00669f

Single-crystal ZnO nanorod/amorphous and nanoporous metal oxide shell composites were facilely prepared by electrochemical deposition and tested as promising electrode materials for supercapacitor applications.

Because of the depleting energy sources and increasing environmental concerns, supercapacitors as alternative energy/power sources have attracted much interest because they have high power density compared to batteries and high energy density compared to conventional capacitors and can be deeply discharged without any deleterious effect on lifetime.[1–3] In this field, designing a new electrode material with high specific capacitance and long-term cycle stability has become one of the most important research focuses.[4,5]

At present, a nanoscale approach to supercapacitor electrode has received great interest because of the unique properties of nanostructures leading to the improved performances.[6] One dimensional (1D) nanostructures have been widely studied because they can provide short diffusion path lengths for ions, leading to high charge/discharge rates.[7,8] However, one of the challenging issues is to tackle their capacity decay with cycling, resulting from the collapse of nanostructures. In addition, the electronic conductivity of metal oxide is generally poor, and it obviously affects their high performances for supercapacitor applications. In order to overcome the above shortcomings, carbon-based materials are widely utilized as supports because of their large surface area and high electrical conductivity.[9] Such investigations are intended to balance the cost and the performances of supercapacitors. In addition, the carbon-based supports possibly encounter severe corrosion in the electrochemical window of some metal oxides *via* eqn (1).[10]

$$C + 2H_2O \rightarrow CO_2 + 4H^+ + 4e^- \text{ (0.207 V } \textit{vs.}\text{ NHE, 25 °C)} \quad (1)$$

Electrochemical corrosion of carbon-based supports will cause the agglomeration of metal oxides coated on the surfaces of supports. In addition, the corrosion of carbon-based supports will lead to electrically isolated metal oxide particles that are detached from the supports. These effects will result in rapid degradation of the electrochemical performances of metal oxide electrodes. Therefore, it will be desirable to use more robust noncarbon supports to avoid the corrosion of supports and prevent agglomeration of metal oxides.[11] Since 1D single-crystal ZnO nanorod is one of the most attractive functional semiconductor materials and has a small capacity, so it can function as efficient mechanical support and electron conducting pathway because of its high chemical stability, conductivity, and

MOE Laboratory of Bioinorganic and Synthetic Chemistry/School of Chem-istry and Chemical Engineering/Institute of Optoelectronic and Functional Composite Materials, Sun Yat-sen University, Guangzhou, 510275, China. E-mail: ligaoren@mail.sysu.edu.cn; Fax: +86-20-84112245; Tel: +86-20-84110071

† Electronic supplementary information (ESI) available: Experimental section; XRD pattern; SEM images. See DOI: 10.1039/c0ee00669f

Broader context

It is well accepted that the nanostructured electrodes with large specific surface area, amorphous and nanoporous configuration can greatly improve the electrode/electrolyte contact area, shorten the diffusion path of current carriers, and enhance the electron conduction in electrodes. However, the poor electronic conductivity of amorphous and nanoporous metal oxides usually affects their high performances in supercapacitors. Based on the above considerations, in this paper, a simple, quick, and general approach was developed for the synthesis of novel composites of single-crystal ZnO nanorod/amorphous and nanoporous metal oxide shells with network structures for supercapacitor applications. The single-crystal ZnO nanorod/amorphous and nanoporous MnO_2 shell composites showed high specific capacitance and long-term cycle ability coupled with low cost and an environmentally benign nature, which will make this material highly attractive for large-scale applications. The results in this paper show an important advancement in the field of the synthesis of novel nanostructured electrode materials for supercapacitors. The novel design idea of this kind of nanostructure is rather universal and very useful to the broader community for synthesizing redox active composite materials.

mechanical flexibility. Here the novel single-crystal ZnO nanorod/amorphous and nanoporous metal oxide shell composites are designed as supercapacitor electrodes because of the added synergic properties or functionalities arising from the combination of different nanomaterials.

MnO_2, with the advantages of environmental friendliness, low cost, and rapid charge-discharge, appears to be a promising electrode material for supercapacitors.[12] However, MnO_2 usually exhibits a low specific capacitance value (100–500 F g^{-1}) that is far from its theoretical value of 1400 F g^{-1}. In this paper, ZnO nanorod/MnO_2 shell composites were synthesized by electrodeposition of amorphous and nanoporous MnO_2 onto the surfaces of ZnO nanorods as illustrated in Fig. 1. The amorphous and nanoporous MnO_2 shells will facilitate ion diffusion and provide high-energy storage capacity. This kind of MnO_2 nanostructure is totally different from those reported before.[13] Here the excellent electrochemical performances of single-crystal ZnO nanorod/amorphous and nanoporous MnO_2 shell composites demonstrate they are the promising electrochemical energy storage materials.

ZnO nanorod precursors were firstly electrodeposited and their SEM images are shown in Fig. 2(a) and (b), which show that the side lengths of hexagonal ZnO nanorods are about 200 nm. The lengths of ZnO nanorods are about 1.5 μm. HRTEM, SAED, and XRD results shown in Fig. S1† indicate that ZnO nanorod has a single crystal structure and a preferential growth in the [0001] direction. Here the prepared ZnO nanorods were employed as precursors, and single-crystal ZnO nanorod/amorphous and nanoporous MnO_2 shell composites were prepared by the electrochemical deposition of Mn onto the surfaces of ZnO nanorods in a solution of 0.01 M $Mn(CH_3COO)_2$ at −0.58 V for 8 min and then heat treatment at 150 °C in atmosphere for 180 min. SEM images of the prepared ZnO nanorod/MnO_2 shell composites with different magnifications are shown in Fig. 2(c) and (d), which show that ZnO nanorods have uniform MnO_2 wraps. The formation of MnO_2 in this study is illustrated as follows:

$$Mn(II)+2e \rightarrow Mn \text{ (Electro-reduction)} \quad (2)$$

$$Mn + O_2 \rightarrow MnO_2 \text{ (Heat treatment at 150 °C in atmosphere)} \quad (3)$$

Furthermore, the MnO_2 wraps favorably share the surface of ZnO nanorods, and no MnO_2 is packed in the interspaces of the nanorods, which suggests MnO_2 is preferentially deposited on the surfaces of ZnO nanorods. TEM images directly confirm the core-shell structures in samples as shown in Fig. 2(e,f). The outer symmetric MnO_2 shell in Fig. 2(e) indicates the uniform wrap, which is about 120 nm in thickness. The magnified TEM image of ZnO nanorod/MnO_2 shell composites is shown in Fig. 2(f), which shows that the MnO_2 shell has nanoporous structures. As we all know, the nanoporous structure can facilitate ion diffusion and has a big surface area. In addition, the network structures in MnO_2 shells are clearly observed as shown in Fig. 2f, and they will benefit electron conduction, which is also an important factor that determines the electrochemical performances. The above advantages are very favorable for high electrochemical properties.

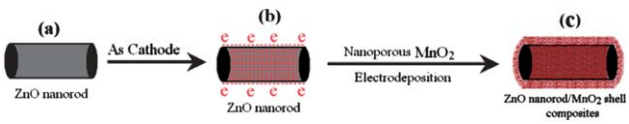

Fig. 1 Schematic illustration of the synthesis of ZnO nanorod/amorphous and nanoporous MnO_2 shell composites.

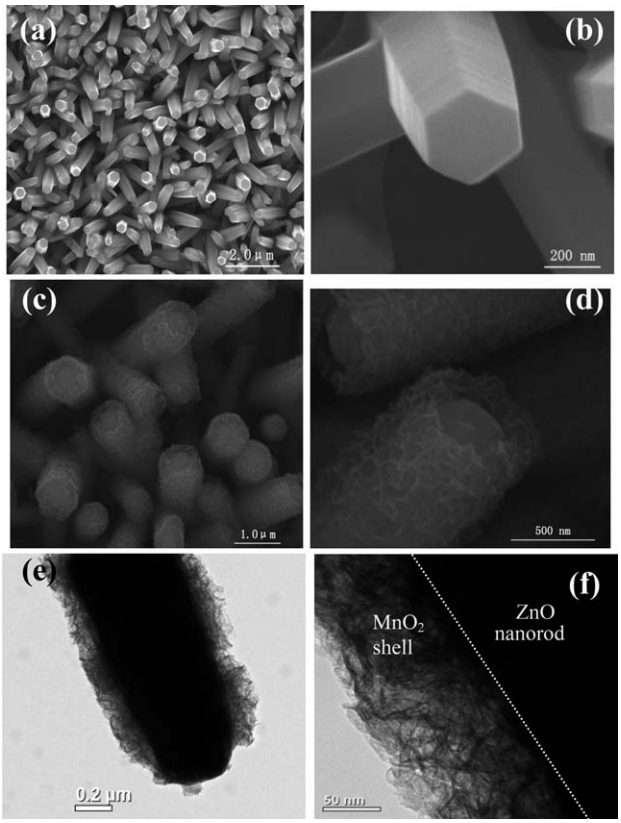

Fig. 2 SEM images of (a,b) ZnO nanorods and (c,d) ZnO nanorod/MnO_2 shell composites with different magnifications; (e,f) TEM images of ZnO nanorod/MnO_2 shell composites with different magnifications.

Fig. 3(a) and (b) show XPS spectra of ZnO nanorod/MnO_2 shell composites in the energy regions of Mn2p and Zn2p, respectively. In Fig. 3(a), the two detected peaks at the binding energies of 641.9 eV and 653.1 eV can be attributed to Mn $2p_{3/2}$ and Mn $2p_{1/2}$, respectively, indicating that element Mn in the prepared samples is present in the chemical state of Mn(IV).[14] The XPS spectrum of Zn 2p3/2 is displayed in Fig. 3(b), and the peak located at 1022.1 eV corresponds to Zn(II) species.[15] Therefore, the above results show the existence of MnO_2 and ZnO in the deposits. Fig. 4 shows the XRD pattern of the prepared ZnO nanorod/MnO_2 shell composites, and it is similar to the XRD pattern of pure ZnO nanorods (Fig. S1(b)†). Besides the peaks of ZnO nanorods and Ti substrate, no MnO_2 peak is observed.

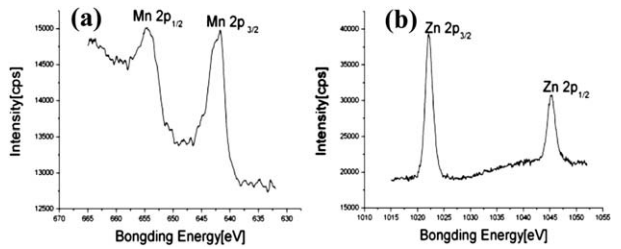

Fig. 3 XPS spectra of ZnO nanorod/MnO_2 shell composites in the energy regions of (a) Mn(2p) and (b) Zn(2p).

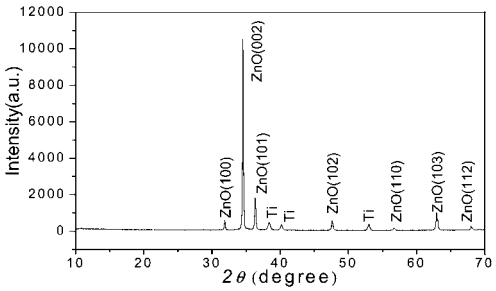

Fig. 4 XRD pattern of ZnO nanorod/MnO_2 shell composites.

This result shows that MnO_2 shells covering the ZnO nanorods are amorphous. The Raman spectrum of ZnO nanorod/MnO_2 shell composites also demonstrates that MnO_2 shells are amorphous, as shown in Fig. S2.†

In this study the thickness of the MnO_2 shell can be well controlled. Hence, this will provide us with the ability to tune the electrochemical properties of ZnO nanorod/MnO_2 shell composites. Since the growth of deposits increases with deposition time, the different MnO_2 shell thicknesses can be obtained at different times as shown in Fig. 5(a)–(d). When the electrodeposition time is 2 min, the MnO_2 shells are uniformly coated on the lateral surfaces of ZnO nanorods as shown in Fig. 5(b), and their thicknesses are about 30 nm. When the deposition time is 3 min, ZnO nanorods can also be completely and uniformly coated on the whole surfaces without MnO_2 filling in the interspaces of the nanorods, as shown in Fig.5(c), with MnO_2 shell thickness of about 45 nm. However, when the electrodeposition time is over 15 min, MnO_2 will cram into the interspaces among ZnO nanorods, meaning it is not uniformly coated on the surfaces of ZnO nanorods, as shown in Fig. 5(d). When the channels or gaps between ZnO nanorods are blocked, this case will significantly increase the resistance of ion diffusion to the electrodes. Fig. 5(e)–(h) show TEM images of MnO_2 shell thickness at different deposition time, and Fig. 5(i) shows the curve of shell thickness as a function of growth time, indicating that the MnO_2 shell can be well controlled by simply adjusting deposition time.

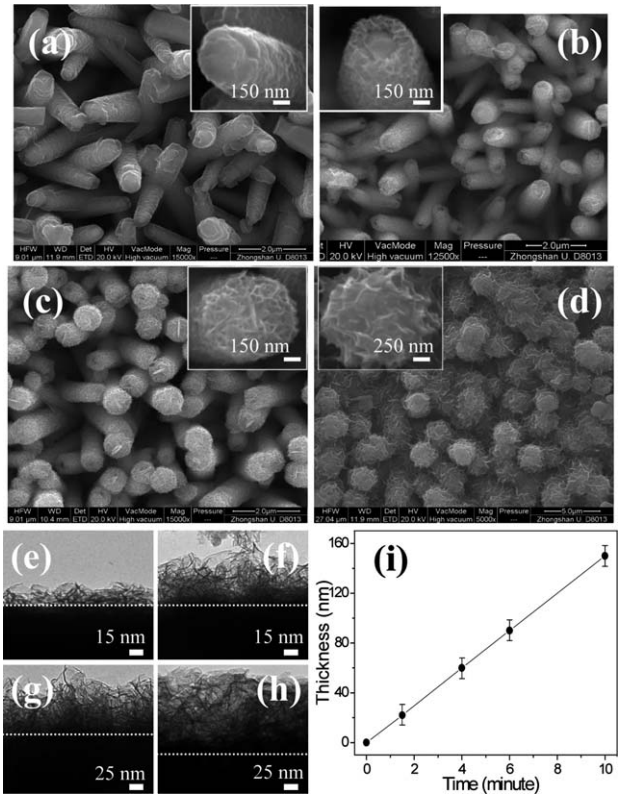

Fig. 5 SEM images of ZnO nanorod/MnO_2 shell composites with different MnO_2 shell thicknesses prepared with different deposition times: (a) 30 s; (b) 2 min; (c) 3 min; (d) 15 min. TEM images of the different shell thicknesses at different growth times: (e) 1.5 min; (f) 4 min; (g) 6 min; (h) 10 min. (i) The curve of shell thickness *vs.* growth time.

The supercapacitive performance of ZnO nanorod/MnO_2 shell composites was studied by the means of cyclic voltammetry (CV). Fig. 6(a)(1) shows CV curve of the ZnO nanorod/MnO_2 shell composite electrode in 1.0 M Na_2SO_4 solution at a scan rate of 10 mV s^{-1}. The specific capacitance (C_{sp}) can be calculated by dividing the capacitance by the weight of samples, namely:

$$C_{sp} = \frac{1}{w\Delta V}\int_y^x i\,dt \quad (4)$$

where i is the current density, t is the time, x is the time when $V = -0.1$ V, y is the time when $V = 0.5$ V, ΔV is the voltage range, and w is the weight of the samples. The C_{sp} of ZnO nanorod/MnO_2 shell composites is calculated to be about 405 F g^{-1} and the C_{sp} of amorphous and nanoporous MnO_2 shells is about 675 F g^{-1} at a scan rate of 10 mV s^{-1}. Fig. 6(a)(2) shows the CV curve of the MnO_2 nanotube electrode in 1.0 M Na_2SO_4 solution at a scan rate of 10 mV s^{-1} (SEM image of MnO_2 nanotubes is shown in Fig. 6(d)). For MnO_2 nanotubes, the C_{sp} is calculated to be about 236 F g^{-1} at a scan rate of 10 mV s^{-1}, much smaller than 405 F g^{-1} of ZnO nanorod/MnO_2 shell composites and 675 F g^{-1} of MnO_2 shells. This can be attributed to the special roles of the inner ZnO nanorod cores, which can function as efficient electron-conducting pathways and mechanical supports, and amorphous and nanoporous MnO_2 shells, which can obviously increase the active sites, improve the homogeneity of electrochemical reaction, and reduce the ionic resistance.

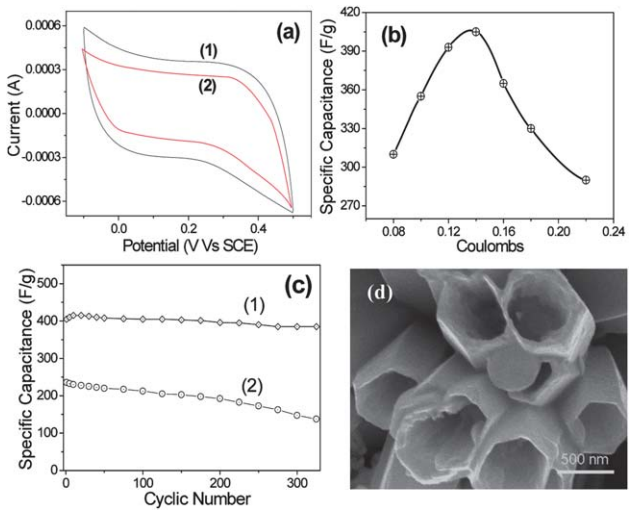

Fig. 6 (a) CV curves of (1) ZnO nanorod/MnO_2 shell composites and (2) MnO_2 nanotubes at 10 mV s^{-1}. (b) Specific capacitance of ZnO nanorod/MnO_2 shell composites *vs.* charge consumed at 10 mV s^{-1}. (c) The variation of specific capacitance as a function of cycle number at 10 mV s^{-1} for (1) ZnO nanorod/MnO_2 shell composites and (2) MnO_2 nanotubes. (d) SEM image of MnO_2 nanotubes.

Fig. 6(b) shows C_{sp} of ZnO nanorod/MnO_2 shell composites *vs.* charge consumed during the electrodeposition of MnO_2. As we all know, the consumed charge is directly proportional to the thickness of the MnO_2 shell (or weight of MnO_2), so this figure will illustrate the trend that the C_{sp} value varies according to the weight of the deposited MnO_2, and it can tell us how to take full advantage of the surfaces of ZnO nanorods. As shown in Fig. 6(b), the C_{sp} value increases at first and then decreases with increasing consumed charge. The peak in this curve shows the optimized C_{sp} of ZnO nanorod/MnO_2 shell composites corresponding to a charge of 0.14 coulombs, which corresponds to a MnO_2 shell thickness of about 90 nm. At this time, amorphous and nanoporous MnO_2 shells are uniformly coated on the surfaces of ZnO nanorods including the top surfaces. Furthermore, no MnO_2 deposit is packed in the interspaces among ZnO nanorods. When the consumed charge further increases, the C_{sp} value will decrease as MnO_2 is crammed into the interspaces of ZnO nanorods, resulting in low usage efficiency.

The electrochemical stability of ZnO nanorod/MnO_2 shell composites was examined by a large number of CV cycles. The variation of C_{sp} value of ZnO nanorod/MnO_2 shell composites as a function of cycle number is shown in Fig. 6(c)(1). It is clearly observed there is an obvious increase in the C_{sp} value in the first 20 cycles and then there is a slight decrease up to 300 cycles. As revealed from the above data, this system can almost withstand over 300 cycles without any significant decrease in C_{sp} value. Therefore, ZnO nanorod/MnO_2 shell composites as supercapacitor electrode show high electrochemical stability for long-term supercapacitor applications. However, for MnO_2 nanotubes, an obvious attenuation is observed as shown in Fig. 6(c)(2).

To demonstrate the universality of the reported method for the enhancement of electrochemical performances of metal oxide, single-crystal ZnO nanorod/amorphous and nanoporous NiO shell composites are also designed as supercapacitor electrodes. NiO has been considered as a good candidate for supercapacitor electrode.[16] SEM image of ZnO nanorod/NiO shell composites is shown in Fig S5.† The thicknesses of amorphous and nanoporous NiO shells are controlled to be about 80 nm. The XRD pattern in Fig. S6† shows that NiO shells on ZnO nanorods are amorphous. Fig. 7(a)(1) shows the CV curve of ZnO nanorod/amorphous and nanoporous NiO shell composite electrode in 0.1 M Na_2SO_4 solution at a scan rate of 10 mV s^{-1}; the C_{sp} value is calculated to be about 305 F g^{-1}, which is much higher than 198 F g^{-1} of NiO nanotubes calculated from Fig. 7(a)(2) (SEM image of NiO nanotubes is shown in Fig. S7†). These prepared ZnO nanorod/amorphous and nanoporous NiO shell composite electrodes also show high electrochemical stability as shown in Fig. 7(b)(1). However, an obvious attenuation is observed for NiO nanotubes as shown in Fig. 7(b)(2), which further proves the positive role of ZnO nanorods for performance enhancement of supercapacitor.

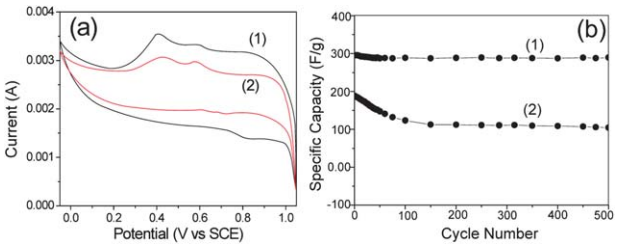

Fig. 7 (a) CV curves of (1) ZnO nanorod/NiO shell composites and (2) NiO nanotubes in 0.1 M Na_2SO_4 at 10 mV s^{-1}. (b) The variation of specific capacitance as a function of cycle number: (1) ZnO nanorod/NiO shell composites and (2) NiO nanotubes.

In summary, a simple and quick approach to novel single-crystal ZnO nanorod/amorphous and nanoporous metal oxide shell composites has been developed for supercapacitor applications. The single-crystal ZnO nanorods as cores experience less structural stress or damage during electrochemical cycling, and they serve as mechanical supports and effective electron transport pathways and increase the electrochemical utilization of metal oxide. The amorphous and nanoporous metal oxide shells obviously increase the active sites, improve the homogeneity of electrochemical reaction, and reduce the ionic resistance. These prepared single-crystal ZnO nanorod/amorphous and nanoporous MnO_2 shell composites have been successfully employed as supercapacitor electrodes and give a high specific capacitance (405 F g^{-1}) at 10 mV s^{-1}. The high specific capacitance and long-term cycle ability coupled with the low cost and environmentally benign nature of ZnO nanorod/MnO_2 shell composites will make this material attractive for large-scale applications. It is believed that the design route of single-crystal ZnO nanorods/amorphous and nanoporous metal oxide shell composites will provide a valuable route for the synthesis of high performance electrode materials for supercapacitor applications.

This work was supported by NSFC (21073240, 20603048, 20873184, and 90923008), Guangdong Province (2008B0106-00040 and 9251027501000002), and the Fundamental Research Funds for the Central Universities (11lgzd14).

Note added after first publication

This article replaces the version published on 25th February 2011, which contained errors in eqn (4).

Notes and references

1 (*a*) C.-M. Yang, Y.-J. Kim, M. Endo, H. Kanoh, M. Yudasaka, S. Iijima and K. Kaneko, *J. Am. Chem. Soc.*, 2007, **129**, 20–21; (*b*) C. Largeot, C. Portet, J. Chmiola, P.-L. Taberna, Y. Gogotsi and P. Simon, *J. Am. Chem. Soc.*, 2008, **130**, 2730–2731; (*c*) D. Hulicova-Jurcakova, A. M. Puziy, O. I. Poddu-bnaya, F. Suárez-García, J. M. D. Tascón and G. Q. Lu, *J. Am. Chem. Soc.*, 2009, **131**, 5026–5027; (*d*) X. Liu and P. G. Pickup, *Energy Environ. Sci.*, 2008, **1**, 494–500; (*e*) T.-Y. Wei, C.-H. Chen, H.-C. Chien, S.-Y. Lu and C.-C. Hu, *Adv. Mater.*, 2010, **22**, 347–351.

2 (*a*) S. W. Lee, B.-S. Kim, S. Chen, Y. Shao-Horn and P. T. Hammond, *J. Am. Chem. Soc.*, 2009, **131**, 671–679; (*b*) T. Brezesinski, J. Wang, S. H. Tolbert and B. Dunn, *Nat. Mater.*, 2010, **9**, 146–151; (*c*) T. Brezesinski, J. Wang, J. Polleux, B. Dunn and S. H. Tolbert, *J. Am. Chem. Soc.*, 2009, **131**, 1802–1809; (*d*) K. Brezesinski, J. Wang, J. Haetge, C. Reitz, S. O. Steinmueller, S. H. Tolbert, B. M. Smarsly, B. Dunn and T. Brezesinski, *J. Am. Chem. Soc.*, 2010, **132**, 6982–6990; (*e*) M. Kaempgen, C. K. Chan, J. Ma, Y. Cui and G. Gruner, *Nano Lett.*, 2009, **9**, 1872–1876.

3 (*a*) A. T. Chidembo, K. I. Ozoemena, B. O. Agboola, V. Gupta, G. G. Wil-dgoose and R. G. Compton, *Energy Environ. Sci.*, 2010, **3**, 228–236; (*b*) C. Peng, S. Zhang, X. Zhou and G. Z. Chen, *Energy Environ. Sci.*, 2010, **3**, 1499–1502; (*c*) H. Ji, Y. Mei and O. G. Schmidt, *Chem. Commun.*, 2010, **46**, 3881–3883; (*d*) C. Liu, F. Li, L.-P. Ma and H.-M. Cheng, *Adv. Mater.*, 2010, **22**, E28–E62; (*e*) Y. Zeng, R. Hao, B. Xing, Y. Hou and Z. Xu, *Chem. Commun.*, 2010, **46**, 3920–3922; (*f*) P. J. Hall, M. Mirzaeian, S. I. Fletcher, F. B. Sillars, A. J. R. Rennie, G. O. Shitta-Bey, G. Wilson, A. Cruden and R. Carter, *Energy Environ. Sci.*, 2010, **3**, 1238–1251.

4 (*a*) A. S. Arico, P. Bruce, B. Scrosati, J. M. Tarascon and W. Van Schalkwijk, *Nat. Mater.*, 2005, **4**, 366–377; (*b*) W. Sugimoto, H. Iwata, Y. Yasunaga, Y. Murakami and Y. Takasu, *Angew. Chem., Int. Ed.*, 2003, **42**, 4092–4096; (*c*) Y.-G. Wang, H.-Q. Li and Y.-Y. Xia, *Adv. Mater.*, 2006, **18**, 2619–2623; (*d*) H. Zhang, G. Cao and Y. Yang, *Energy Environ. Sci.*, 2009, **2**, 932–943; (*e*) N. A. Choudhury, S. Sampath and A. K. Shukla, *Energy Environ. Sci.*, 2009, **2**, 55–67; (*f*) M. M. Shaijumon, F. S. Ou, L. Ci and P. M. Ajayan, *Chem. Commun.*, 2008, 2373–2375.

5 (*a*) C.-C. Hu, K.-H. Chang, M.-C. Lin and Y. T. Wu, *Nano Lett.*, 2006, **6**, 2690–2695; (*b*) C. Xu, Y. Zhao, G. Yang, F. Li and H.-L. Li, *Chem. Commun.*, 2009, 7575–7577; (*c*) L. Cao, F. Xu, Y. Liang and H.-L. Li, *Adv. Mater.*, 2004, **16**, 1853–1857; (*d*) H. Liu, L.-H. Jin, P. He, C. Wang and Y.-Y. Xia, *Chem. Commun.*, 2009, 6813–6815; (*e*) Y. Wang, H. Li and Y.-Y. Xia, *Adv. Mater.*, 2006, **18**, 2619–2623.

6 (*a*) D. Choi, G. E. Blomgren and P. N. Kumta, *Adv. Mater.*, 2006, **18**, 1178–1182; (*b*) G. Wee, H. Z. Soh, Y. L. Cheah, S. G. Mhaisalkar and M. Srinivasan, *J. Mater. Chem.*, 2010, **20**, 6720–6725; (*c*) Y.-F. Lee, K.-H. Chang, C.-C. Hu and K.-M. Lin, *J. Mater. Chem.*, 2010, **20**, 5682–5688; (*d*) H. Yu, X. Fu, C. Zhou, F. Peng, H. Wang and J. Yang, *Chem. Commun.*, 2009, 2408–2410.

7 (*a*) P. Simon and Y. Gogotsi, *Nat. Mater.*, 2008, **7**, 845–854; (*b*) O. N. Kalugin, V. V. Chaban, V. V. Loskutov and O. V. Prezhdo, *Nano Lett.*, 2008, **8**, 2126–213; (*c*) J. Yan, E. Khoo, A. Sumboja and P. S. Lee, *ACS Nano*, 2010, **4**, 4247–4255.

8 (*a*) R. Liu and S. B. Lee, *J. Am. Chem. Soc.*, 2008, **130**, 2942–2943; (*b*) Y. Liang, X. Feng, L. Zhi, U. Kolb and K. Müllen, *Chem. Commun.*, 2009, 809–811; (*c*) H. Pang, Q. Lu, Y. Li and F. Gao, *Chem. Commun.*, 2009, 7542–7544.

9 (*a*) R. K. Sharma, H.-S. Oh, Y.-G. Shul and H. Kim, *Phys. B*, 2008, **403**, 1763–1769; (*b*) A. E. Fischer, K. A. Pettigrew, D. R. Rolison, R. M. Stroud and J. W. Long, *Nano Lett.*, 2007, **7**, 281–286.

10 (*a*) K. Kinoshita, *Carbon: Electrochemical and Physicochemical Proper-ties*; Wiley: New York, 1988, p 319; (*b*) S.-Y. Huang, P. Ganesan, S. Park and B. N. Popov, *J. Am. Chem. Soc.*, 2009, **131**, 13898–13899.

11 (*a*) C.-C. Hu, H.-Y. Guo, K.-H. Chang and C.-C. Huang, *Electrochem. Commun.*, 2009, **11**, 1631–1634; (*b*) C.-C. Hu, C.-Y. Hung, K.-H. Chang and Y.-L. Yang, *J. Power Sources*, 2011, **196**, 847–850; (*c*) G.-R. Li, Z.-L. Wang, F.-L. Zheng, Y.-N. Ou and Y.-X. Tong, *J. Mater. Chem.*, 2011, **21**, DOI: 10.1039/C0JM03500A.

12 (*a*) Z.-S. Wu, W. Ren, D.-W. Wang, F. Li, B. Liu and H.-M. Cheng, *ACS Nano*, 2010, **4**, 5835–5842; (*b*) M. Toupin, T. Brousse and D. Bélanger, *Chem. Mater.*, 2004, **16**, 3184–3190; (*c*) A. J. Roberts and R. C. T. Slade, *J. Mater. Chem.*, 2010, **20**, 3221–3226.

13 (*a*) C.-C. Hu and C.-C. Wang, *J. Electrochem. Soc.*, 2003, **150**, A1079; (*b*) M.-S. Wu and P.-C. J. Chiang, *Electrochem. Solid-State Lett.*, 2004, **7**, A123; (*c*) H. Zhang, G. Cao, Z. Wang, Y. Yang, Z. Shi and Z. Gu, *Nano Lett.*, 2008, **8**, 2664–2668; (*d*) C.-C. Hu, K.-H. Chang, Y.-T. Wu, C.-Y. Hung, C.-C. Lin and Y.-T. Tsai, *Electrochem. Commun.*, 2008, **10**, 1792–1796; (*e*) B. Babakhani and D. G. Ivey, *J. Power Sources*, 2010, **195**, 2110–2117.

14 (*a*) X. F. Xie and L. Gao, *Carbon*, 2007, **45**, 2365–2373; (*b*) C. Zhou, H. Wang, F. Peng, J. Liang, H. Yu and J. Yang, *Langmuir*, 2009, **25**, 7711–7717.

15 G.-R. Li, X.-H. Lu, C.-Y. Su and Y.-X. Tong, *J. Phys. Chem. C*, 2008, **112**, 2927–2933.

16 (*a*) J.-H. Kim, K. Zhu, Y. Yan, C. L. Perkins and A. J. Frank, *Nano Lett.*, 2010, **10**, 4099–4104; (*b*) C. Z. Yuan, X. G. Zhang, L. H. Su, B. Gao and L. F. Shen, *J. Mater. Chem.*, 2009, **19**, 5772–5777; (*c*) J. W. Lang, L. B. Kong, W. J. Wu, Y. C. Luo and L. Kang, *Chem. Commun.*, 2008, 4213–4215.

